

Relationship between structural phase transitions and elastic anomalies in metallic superlattices

Eric E. Fullerton^{a)} and Ivan K. Schuller

Physics Department, University of California, San Diego, La Jolla, California 92093-0319

F. T. Parker

Center for Magnetic Recording Research, University of California, San Diego, La Jolla, California 92093-0401

Kathryn A. Svinarich

Department of Physics and Astronomy, Wayne State University, Detroit, Michigan 48202

Gary L. Eesley

Physics Department, General Motors Research Laboratories, Warren, Michigan 48090-9055

R. Bhadra and M. Grimsditch

Materials Science Division, Argonne National Laboratory, Argonne, Illinois 60439

(Received 20 November 1992; accepted for publication 29 January 1993)

A detailed study of the structural and elastic properties of Fe/Cu superlattices has been performed. These superlattices exhibit a structural phase transition as a function of layer thickness in which bcc α -Fe transforms into fcc γ -Fe. This structural phase transition in which the Fe layers become coherent with the Cu layers is signaled by clear-cut changes in elastic and magnetic properties. The elastic properties studied through this transition indicate that in-plane coherency plays an important role in the elastic behavior of metallic superlattices.

I. INTRODUCTION

Understanding the mechanical properties of metallic superlattices and multilayers has been a challenging experimental and theoretical problem.¹ The current, generally accepted, experimental conclusion is that elastic anomalies are present in metallic superlattices. These anomalies, although not as striking as those in the original report,² nevertheless are much larger than any predictions based on simple continuum elasticity theory. In almost all cases the elastic anomalies, which may typically be of the order of 10%–50%,^{3–9} are correlated with structural lattice expansions and contractions of the order of 2%–4%.^{5,7,9,10} The origin of the observed structural expansions is not well understood at the present time.

A number of theoretical models have been advanced to explain the origin of the elastic anomalies. In general these theoretical explanations can be divided into two categories: electronic or structural. Electronic explanations have attributed the presence of elastic anomalies either to changes in the Fermi surface due to the added periodicity of the superlattice^{11–13} or to charge transfer across the interfaces.^{14,15} Structural explanations attribute the elastic anomalies to strains present at the interfaces.^{16–22} Numerical simulations that use the experimentally measured expansions are able to quantitatively fit the elastic anomalies.^{17,22} To date, however, no comprehensive theory has emerged that simultaneously describes the structural and the elastic anomalies. Although a first step in this direction is the “grain-boundary” model,^{20,21} a quantitative theory

applicable to the different structures experimentally investigated has not yet emerged.

Experimentally, it is clear that the elastic and structural anomalies are correlated. It is therefore important to explore this fact in systems in which precise structural and mechanical measurements are performed. We present here a detailed study of both structural and mechanical characteristics of Fe/Cu superlattices. Since it is known that Fe can exist in a variety of epitaxial phases which are determined by the growth conditions, this is an ideal system in which to study the relationship between structure and elastic properties. More specifically, it has already been shown that in a superlattice Fe undergoes a structural phase transition from bcc α -Fe to fcc γ -Fe which depends on the thicknesses of the Fe and Cu layers.^{23–27}

II. EXPERIMENTAL DETAILS

Fe/Cu superlattices (with either 0.2 or 0.5 μm total thickness) were prepared using magnetron sputtering onto ambient temperature sapphire, mica, and Si substrates as described earlier.²⁸ The thicknesses were determined by precise control of the sputtering rates and by timing the computer-controlled substrate holder. Four series of films in the superlattice wavelength $10 \text{ \AA} < \Lambda < 300 \text{ \AA}$ with nominal relative thicknesses ($t_{\text{Fe}}:t_{\text{Cu}}$) of 3:1, 1:1, 1:2, and 1:3 were prepared.²⁹ To investigate the effect of a buffer layer a series with a 500 \AA Cu underlayer was also fabricated. This buffer layer produces no measurable effect on either the structural or the mechanical properties. Structural studies were performed on a computer-controlled Rigaku D-Max II x-ray diffractometer using $\text{CuK}\alpha$ radiation. Room-temperature magnetization measurements were performed using a vibrating sample magnetometer and conversion

^{a)}Present address: Materials Science Division, Argonne National Laboratory, Argonne, IL 60439.

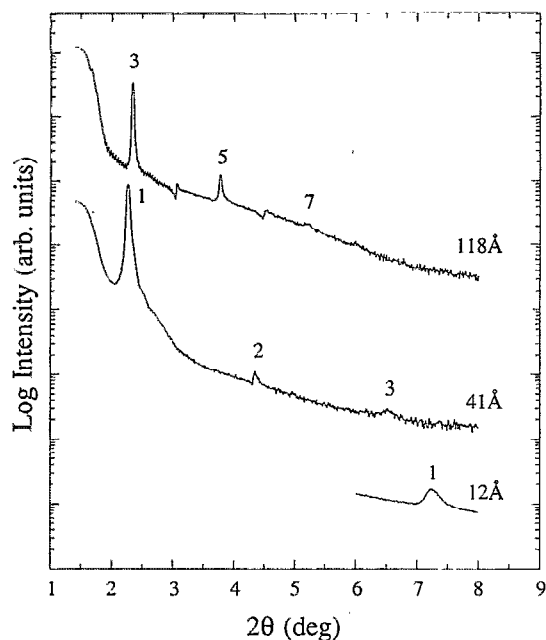


FIG. 1. Low-angle θ - 2θ x-ray-diffraction spectra for representative 1:1 Fe/Cu superlattices. Spectra are offset for clarity. Numbers indicate the order of the low-angle peaks.

electron Mössbauer spectroscopy (CEMS). Shear elastic constants were measured using Brillouin scattering with a 5+2 tandem Fabry-Perot spectrometer and the perpendicular longitudinal modulus C_{33} was measured using transient piezoreflectance (TPR) measurements.^{30,31}

III. STRUCTURE

Low- and high-angle θ - 2θ and θ (rocking curves) x-ray scans allow a detailed structural characterization of the samples. Figure 1 shows low-angle θ - 2θ x-ray scans for a representative series of samples. Well-resolved low-angle diffraction peaks were observed for all modulation wavelengths studied indicating a well-defined layered structure. Finite-size peaks which arise from interference of the surface and substrate reflections can be seen in about the third-order reflection of the $\Lambda = 118$ Å film.

High-angle x-ray results are similar to those observed by a number of groups.²³⁻²⁶ For large modulations, $\Lambda > 200$ Å, Cu(111) and α -Fe bcc(110) peaks are resolved separately, whereas at smaller Λ , a single broad diffraction peak is found at 2θ located between the Cu(111) and α -Fe(110) peaks (Fig. 2). Rocking curves about this peak indicate that the mosaic spread is of the order of 20° . High-angle superlattice satellites are not observed and the Cu(200), Cu(220), and Cu(311) have much smaller intensities than the Cu(111).

The samples with ratios ($t_{\text{Fe}} : t_{\text{Cu}}$) 3:1 and 1:1 exhibit α -Fe growth for all modulations as indicated by the presence of Fe bcc(200) and bcc(211) peaks. However, the samples with the nominal ratio ($t_{\text{Fe}} : t_{\text{Cu}}$) 1:2 and 1:3 show that the intensity of the α -Fe(200) and (211) peaks decreases with decreasing Λ until they disappear in the samples with the lowest modulations. Figure 2 shows the main

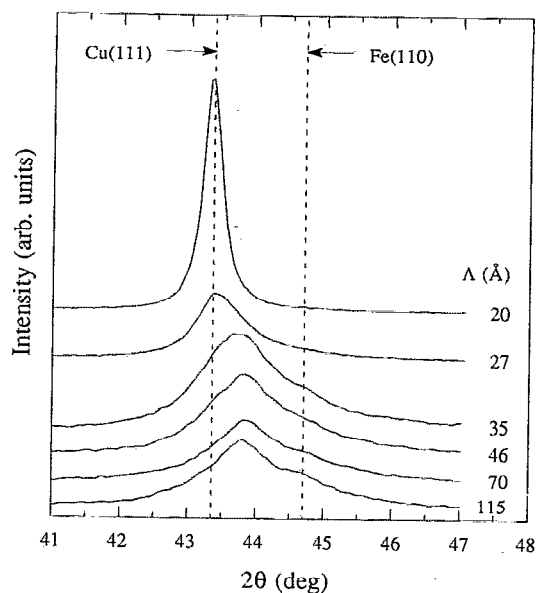


FIG. 2. High-angle θ - 2θ x-ray-diffraction scans of 1:2 samples with scattering vector normal to the superlattice. X-ray spectra are offset for clarity. The $\Lambda = 27$ and 20 Å samples' spectra are reduced in intensity by a factor of 5. Dashed lines indicate the expected position of Cu(111) and α -Fe(110) peak positions.

diffraction peak for a series of samples with nominal ratios ($t_{\text{Fe}} : t_{\text{Cu}}$) 1:2. As in the case for the other thickness ratios, a single diffraction peak is observed intermediate between the expected Cu(111) and the α -Fe(110) peaks. The peak position and its shape are independent of Λ down to $\Lambda \approx 35$ Å. For smaller Λ , the θ - 2θ peak and the rocking curve sharpen and the diffraction peak shifts toward the Cu(111) position indicating that a structural transition has taken place in the superlattice. These changes occur in the region of Λ where the α -Fe bcc(200) and (211) lines disappear and the bcc α -Fe peaks were found to be absent in transmission x-ray scans of the $\Lambda = 20$ Å sample. The coherence length extracted from the width of the high-angle diffraction line is greater than 10Λ . A similar shift and sharpening of the high-angle diffraction peak is observed for the 1:3 samples near the same Fe layer thickness.

For the 1:2 $\Lambda = 20$ and 115 Å samples, the θ - 2θ scan along the expected bcc(211) and fcc(311) directions (scattering angle of 29.7° with respect to the film normal) is shown in Fig. 3. In the $\Lambda = 115$ Å sample both the α -Fe bcc(211) and Cu fcc(311) are observed. The bcc(211) peak at the expected α -Fe position is absent in the $\Lambda = 20$ Å sample and a sharp peak is observed at the expected Cu(311) position with a linewidth of $\approx 1.5^\circ$. This linewidth translates into a coherence length larger than 75 Å along the fcc(311) direction which extends over many layers and is clear evidence for a coherent fcc structure of the Cu and Fe layers in this superlattice. If the growth were not coherent (i.e., bcc Fe on fcc Cu), the coherence length would be limited by the finite thickness of the individual layers since the fcc(111) and bcc(110) planes have different rotational symmetries and are incoherent along the bcc(211)-fcc(311) directions.

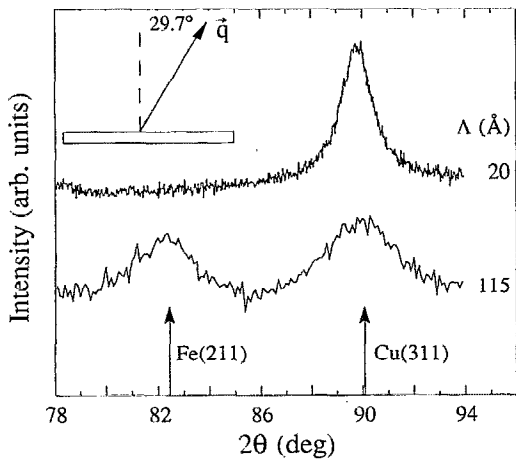


FIG. 3. High-angle θ - 2θ x-ray-diffraction scans of 1:2 samples for $\Lambda=20$ and 115 \AA with the scattering vector at 29.7° relative to the film normal. Arrows indicate expected positions of α -Fe(211) and Cu(311) peaks. These peaks are expected at 30° and 29.5° with respect to the film normal, respectively, and should both be observable.

Figure 4 shows the perpendicular average lattice parameter \bar{d} extracted directly from the central peak position of the high-angle diffraction data. All samples with ratios ($t_{\text{Fe}}:t_{\text{Cu}}$) 3:1 and 1:1 show only slight changes in \bar{d} as a function of Λ , whereas the samples with the ratio 1:2 and 1:3 show little change down to the thickness at which the bcc α -Fe to fcc γ -Fe occurs. At this thickness, the structural phase transition is signaled by an expansion in which the average lattice spacing becomes almost equal to the bulk Cu lattice parameter.

The structural results presented above are indicative of a phase transition of the Fe layers in superlattices with $t_{\text{Cu}} > 1.5t_{\text{Fe}}$ and for $t_{\text{Fe}} < 12 \text{ \AA}$. The results are consistent with previous reports of the presence of fcc γ -Fe in Fe/Cu superlattices.²³⁻²⁷

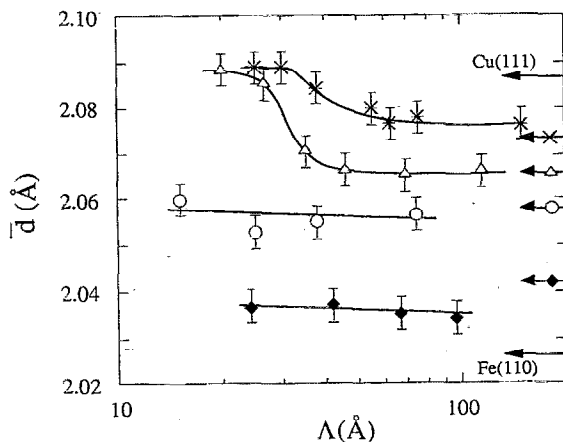


FIG. 4. Perpendicular average lattice spacing \bar{d} as a function of Λ for different ratios $t_{\text{Fe}}:t_{\text{Cu}}$. (\blacklozenge) 3:1; (\circ) 1:1; (Δ) 1:2; and ($*$) 1:3. Arrows indicate the expected peak positions of bulk Fe(110) and Cu(111) and superlattice positions.

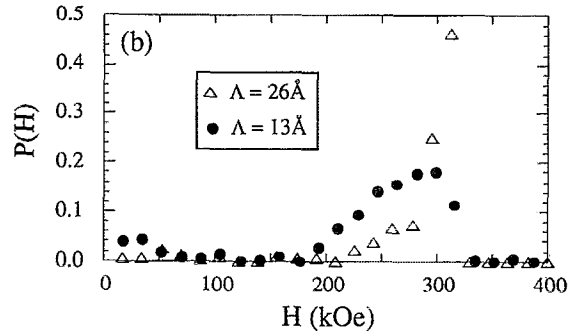
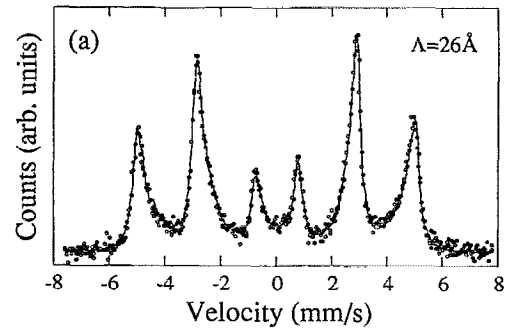


FIG. 5. CEMS results on 1:1 Fe/Cu superlattices. (a) Measured spectrum (circles) for $\Lambda=26 \text{ \AA}$ sample and fit to a distribution of hyperfine fields (line). (b) Distribution of hyperfine field $P(H)$ vs hyperfine field H determined from fitting the measured Mössbauer spectra for $\Lambda=26 \text{ \AA}$ and $\Lambda=13 \text{ \AA}$.

IV. MÖSSBAUER RESULTS

To study the local environment of the Fe atoms, three superlattices were studied by CEMS. Shown in Fig. 5(a) is the measured CEMS spectra for an Fe(13 \AA)/Cu(13 \AA) superlattice measured at room temperature and zero applied field. The spectrum consists of the expected magnetically split six lines. The magnetic splitting is most dependent on the nearest-neighbor (nn), and next-nearest-neighbor (nnn) environment of the Fe atoms. The Fe atoms with one or more Cu nn or nnn will have a reduced hyperfine field relative to the value of the atoms with all Fe neighbors. The CEMS spectra were fit with a superposition of six line subspectra which have a distribution of hyperfine fields H . The isomer shift of each subspectrum was fit as an independent parameter. Quadrupole splitting and relative line broadening were ignored. The fit of a CEMS spectrum generates a $P(H)$ plot, where $P(H)$ is the relative height of a subspectra with hyperfine field H . Each $P(H)$ distribution is normalized, so that the sum of the $P(H)$ values equals one.

Shown in Fig. 5(b) are the results of fitting the CEMS spectra to a distribution of hyperfine fields for 1:1 samples with $\Lambda=26 \text{ \AA}$ and $\Lambda=13 \text{ \AA}$. The resulting $P(H)$ curve for the $\Lambda=26 \text{ \AA}$ sample shows a sharp peak at $H=315 \text{ kOe}$, which corresponds to the Fe atoms with all Fe nn and nnn. This value is slightly reduced compared to the bulk Fe value ($H=330 \text{ kOe}$) and has been observed in other Fe/Cu superlattices.^{32,33} The contribution of the Fe atoms near the interface which have some Cu neighbors gives rise

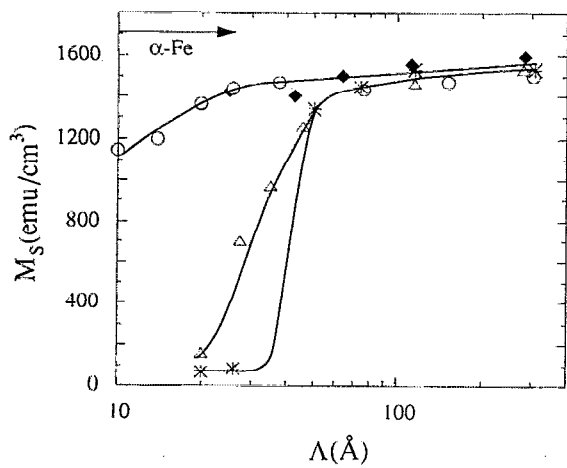


FIG. 6. Room-temperature saturation magnetization M_s vs Λ for different ratios of $t_{\text{Fe}}:t_{\text{Cu}}$: (\blacklozenge) 3:1; (\circ) 1:1; (\triangle) 1:2; and ($*$) 1:3. The arrow indicates the bulk Fe moment.

to the tail at lower H in the $P(H)$ curve. For an Fe thickness of 13 Å (corresponding to ≈ 6.5 monolayers of Fe), if the interface were chemically sharp, then $\approx 40\%$ of the Fe layers will have all Fe nn and nnn. The intensity of the $H=315$ kOe peak is 42% of the spectrum, indicating that there is very little interdiffusion (≈ 1 monolayer) at each interface in agreement with Refs. 23, 32, and 33. When the Fe thickness is decreased to ≈ 7 Å, all the Fe atoms should have at least one Cu nn or nnn. This should result in the disappearance of the peak at 315 kOe which is clearly evident in Fig. 5(b). The fact that $P(315 \text{ kOe})$ is finite may indicate that there are some layer thickness fluctuations giving rise to thicker regions of Fe. The CEMS results also show that less than 10% of the Fe atoms are nonmagnetic. This is direct contrast with the Mössbauer spectrum for the 1:2 Fe/Cu superlattices with ≈ 7 Å Fe layer which has the γ -Fe structure. The room-temperature spectrum is a nonmagnetic, essentially unsplit Mössbauer spectrum in agreement with previous studies.²³

V. MAGNETIC PROPERTIES

Further supporting evidence for the formation of fcc γ -Fe in the 1:2 and 1:3 samples comes from magnetization measurements. The measured room-temperature saturation magnetization M_s of the Fe layer as a function of modulation wavelength is shown in Fig. 6 for the various series of samples. The saturation magnetization for the 3:1 and 1:1 samples is only slightly Λ dependent with M_s close to the value for bulk Fe in agreement with previous measurements.^{32,33} The slight decrease of M_s at lower Fe thicknesses is due to a decreased magnetic contribution of the Fe atoms close to the interface as indicated in the CEMS results. In contrast to the 3:1 and 1:1 samples, the 1:2 and 1:3 superlattices show a sharp drop in magnetization close to the same critical thickness at which the x-ray lines shift. At the smallest modulations, the room-temperature ferromagnetic signal is less than 5% of that expected for α -Fe, indicating that the majority of the Fe has transformed into a nonmagnetic phase in agreement with the Mössbauer

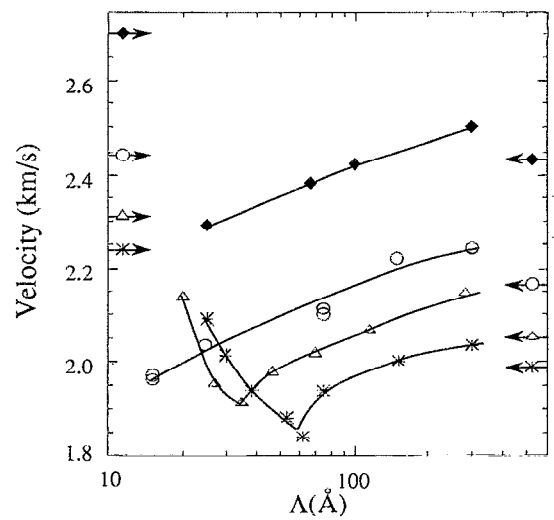


FIG. 7. Surface phonon velocity vs Λ for different ratios of $t_{\text{Fe}}:t_{\text{Cu}}$: (\blacklozenge) 3:1; (\circ) 1:1; (\triangle) 1:2; and ($*$) 1:3.

results. For comparable Fe layer thickness in the 1:1 superlattices, the Fe moment is 70% of the expected moment with less than 10% of the Fe nonmagnetic as determined by CEMS. These results are in agreement with earlier measurements on epitaxial Fe on Cu films^{34,35} and small Fe clusters in a Cu matrix.³⁶ All these earlier measurements indicate that Fe transforms to a nonmagnetic γ -Fe phase below a certain critical thickness or size.

VI. ELASTIC PROPERTIES

Figure 7 shows the surface phonon velocity v measured using Brillouin scattering on superlattices with a total thickness > 5000 Å. The various symbols represent samples from series with different Fe:Cu ratios and the solid lines are guides to the eye. The surface phonon velocity is related to the shear elastic constant C_{44} through³⁷

$$v = \beta \sqrt{C_{44}/\rho}, \quad (1)$$

where ρ is the average mass density of the film, and β ($\approx 0.8-1.0$) is a constant that depends weakly on C_{11} , C_{33} , and C_{13} . The measured velocities can be directly compared to the velocities calculated using continuum elasticity theory.³⁷ The velocities expected for the superlattice calculated using the bulk Fe and Cu elastic moduli³⁸ are shown by the arrows in Fig. 7. Because the samples are polycrystalline in the plane, the elastic constants have to be averaged over all possible in-plane orientations. This gives rise to some uncertainty in the calculated velocity depending on the averaging procedure (Reuss or Voigt).³⁹ The arrows on the right-hand side represent the Reuss average and the arrows on the left-hand side the Voigt.

At large Λ , there is agreement between calculated and measured velocities since the latter are within the calculated range, although closer to the Reuss average values; however, as Λ decreases, the phonon wave velocity initially decreases for all samples. This behavior is similar to that of other immiscible bcc/fcc superlattices.^{3-7,10} The decrease

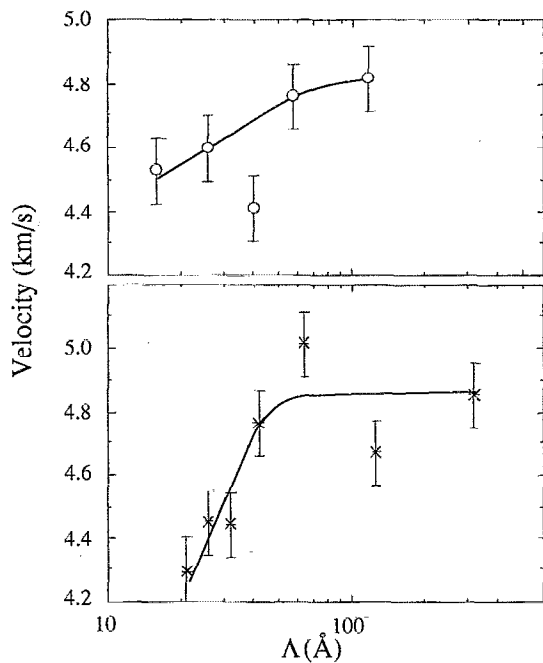


FIG. 8. Longitudinal phonon velocity perpendicular to the layers vs Λ for different ratios of $t_{\text{Fe}}:t_{\text{Cu}}$: (○) 1:1 and (*) 1:3.

in the 1:1 sample phonon velocity is 13% which corresponds to a 25% decrease in C_{44} . Since no major changes are found in the perpendicular lattice spacing this is clearly not the relevant structural parameter which drives the shear elastic constant changes. The most striking results are obtained for the samples with nominal $t_{\text{Fe}}:t_{\text{Cu}}$ ratios 1:2 and 1:3. In this case a minimum develops in the phonon velocity with the minimum coinciding with the thickness at which the α -Fe to γ -Fe transition takes place.

The longitudinal sound velocity measured by TPR is shown in Fig. 8 for the $t_{\text{Fe}}:t_{\text{Cu}}$ ratio 1:3 and 1:1 samples with total thickness of 2000 Å. The longitudinal phonon velocity is related to the elastic constant C_{33} through

$$v = \sqrt{C_{33}/\rho}. \quad (2)$$

We were unable to obtain a measurable signal from the Fe-rich samples due to a lack of sufficient contrast in the density and elastic properties at the film-substrate interface. The behavior of the sound velocity in this case is quite different from the shear velocity described above. The expected longitudinal velocity calculated from the bulk Fe and Cu elastic constants is 5.55 and 5.35 for the 1:1 and 1:3 samples, respectively. The measured velocity of the large Λ samples is lower than the expected values, which may result from the mosaic spread of the crystals. As seen for the surface wave velocity, the 1:1 samples show a slight monotonic drop as Λ decreases. The behavior of the longitudinal velocity in the 1:3 samples is quite different from the surface velocity described above. In the 1:3 samples with large Λ (> 60 Å) the velocities are constant within experimental error. As Λ decreases, the longitudinal velocity sharply drops at the thickness corresponding to the structural phase transition. This behavior is opposite to the $\Lambda < 60$ Å

dependence in the 1:3 sample's surface wave velocity. The decrease in the longitudinal velocity is, however, consistent with the expansion of the perpendicular lattice spacing shown in Fig. 4.⁷

VII. DISCUSSION

A number of conclusions can be drawn from these data that are independent of specific theoretical models, as follows.

(i) Clearly in this system the earlier correlation between perpendicular lattice spacing \bar{d} and phonon velocity is not crucial. The most dramatic changes in \bar{d} are for the 1:2 and 1:3 samples where both \bar{d} and surface phonon velocities increase with decreasing Λ . Therefore, the behavior of the shear modulus cannot simply be assigned to the perpendicular lattice changes or a weakening of the perpendicular bonding.

(ii) The elastic anomalies in Fe/Cu superlattices are strongly correlated with the structural phase transition of the Fe layers. The x-ray studies indicate quite conclusively that the thin layers of Fe (< 12 Å) transform into γ -Fe when the Cu layer is thicker than the Fe layer.

(iii) In the present case, the thin layers which form coherent interfaces (γ -Fe) have a shear modulus close to the value at large Λ (α -Fe) and a longitudinal modulus softened with respect to the large Λ value.

A comparison of our experimental results with the theoretical models of the supermodulus effect is severely hampered by lack of detailed predictions of all but the grain-boundary model.^{20,21} For example, in the electron transfer model¹⁵ it could be argued that the charge transfer drives the bcc-fcc phase transformation and that all elastic anomalies simply reflect this fact. Speculative arguments such as this cannot be either proved or disproved with our current knowledge of these systems and hence they provide no useful insight. We believe that similar arguments could be made for the surface tension model,^{17,18} the zone folding model,¹¹⁻¹³ and perhaps also for the coherency strain model.^{16,17}

Until the above models are able to produce specific predictions, our results can only be compared with the predictions of the grain-boundary model.^{20,21} Even here, however, only a qualitative comparison can be made since the calculations were performed for fcc/fcc superlattices and did not consider structural phase changes. We suggest that the experimental results can be qualitatively understood as a superlattice system that undergoes a coherent-incoherent phase transformation. In Ref. 21 it has been shown that in an incoherent interface superlattice, C_{44} should decrease sharply and C_{33} should change by less than $\approx 3\%$. For the coherent interface case, C_{44} should be almost independent of Λ and C_{33} should decrease by $\approx 12\%$. For samples with no γ -Fe detected (i.e., all 3:1 and 1:1 samples and $t_{\text{Fe}} > 12$ Å in the 1:2 and 1:3 samples) the softening in C_{44} and the small change in C_{33} are consistent with atomic level disorder at an incoherent interface.²¹ For $t_{\text{Fe}} < 12$ Å in the 1:2 and 1:3 samples where γ -Fe is present, the increase in C_{44} and decrease in C_{33} are consistent with the formation of coherent interfaces in which the changes

are produced by the removal of disorder as γ -Fe is formed. If the small Λ samples are indeed perfectly coherent, then these samples should reflect the elastic properties of γ -Fe. Our results would then indicate that C_{44} of γ -Fe is roughly equal to that of α -Fe and C_{33} is somewhat lower.

In conclusion, we have performed a detailed study of the structure and elastic properties of Fe/Cu superlattices. For certain modulation wavelengths and ratios of Fe:Cu thicknesses, these superlattices exhibit a structural phase transition in which bcc α -Fe transforms into fcc γ -Fe. This structural phase transition is signaled by clear cut changes in structural parameters, in the magnetic properties, and in the mechanical properties. Our results are in good agreement with the predictions of the grain-boundary model. However, a clear-cut explanation and a way to properly engineer elastic constants into artificial materials will only arise if theoretical calculations are performed specifically on the same systems that are studied experimentally.

ACKNOWLEDGMENTS

The work was supported by the ONR under Contract No. N00014-91-J-1177 (E.E.F. and I.K.S.), the U.S. Department of Energy, Basic Energy Sciences, Materials Sciences, under Contract No. W31-109-ENG-38 (R.B. and M.G.), and Contract No. NSF-DMR-90-10908 (F.T.P.). We would like to thank M. Carey for assistance in magnetization measurements.

¹For a recent review, see R. G. Brandt, *Mater. Sci. Eng. B* **6**, 95 (1990); I. K. Schuller, A. Fartash, and M. Grimsditch, *MRS Bull.* **15**, 33 (1990); B. Y. Jin and J. B. Ketterson, *Adv. Phys.* **38**, 189 (1989); or M. H. Grimsditch, in "Light Scattering in Solids V," edited by M. Cardona and G. Güntherodt, *Topics in Applied Physics*, Vol. 66 (Springer, New York, 1989).

²W. M. C. Yang, T. Tsakalakos, and J. E. Hilliard, *J. Appl. Phys.* **48**, 876 (1977).

³A. Kueny, M. Grimsditch, K. Miyano, I. Banerjee, C. M. Falco, and I. K. Schuller, *Phys. Rev. Lett.* **48**, 166 (1982).

⁴J. A. Bell, R. J. Zanon, C. T. Seaton, G. I. Stegeman, W. R. Bennett, and C. M. Falco, *Appl. Phys. Lett.* **51**, 652 (1987).

⁵A. Fartash, E. E. Fullerton, I. K. Schuller, S. E. Bobbin, J. W. Wagner, R. C. Cammarata, S. Kumar, and M. Grimsditch, *Phys. Rev. B* **44**, 13 760 (1991).

⁶M. R. Khan, C. S. L. Chun, G. P. Felcher, M. Grimsditch, A. Kueny, C. M. Falco, and I. K. Schuller, *Phys. Rev. B* **27**, 7186 (1983).

⁷B. M. Clemens and G. L. Eesley, *Phys. Rev. Lett.* **61**, 2356 (1988).

⁸J. R. Dutcher, S. Lee, J. Kim, G. I. Stegeman, and C. M. Falco, *Phys. Rev. Lett.* **65**, 1231 (1990).

⁹P. Bisanti, M. B. Brodsky, G. P. Felcher, M. Grimsditch, and L. R. Sill, *Phys. Rev. B* **35**, 7813 (1987).

¹⁰I. K. Schuller and M. Grimsditch, *J. Vac. Sci. Technol. B* **4**, 1444 (1986).

¹¹T. B. Wu, *J. Appl. Phys.* **53**, 5265 (1982).

¹²W. E. Pickett, *J. Phys. F* **12**, 2195 (1982).

¹³R. C. Cammarata, *Scr. Metall.* **20**, 479 (1986).

¹⁴M. Grimsditch, *Superlattices and Microstructures* **4**, 677 (1988).

¹⁵M. L. Huberman and M. Grimsditch, *Phys. Rev. Lett.* **62**, 1403 (1989).

¹⁶A. F. Jankowski, *J. Phys. F* **18**, 413 (1988).

¹⁷A. F. Jankowski, *J. Mater. Sci. Eng. B* **6**, 191 (1991).

¹⁸R. C. Cammarata and K. Sieradzki, *Phys. Rev. Lett.* **62**, 2005 (1989).

¹⁹F. H. Streitz, K. Sieradzki, and R. C. Cammarata, *Phys. Rev. B* **41**, 12 285 (1990).

²⁰D. Wolf and J. F. Lutsko, *Phys. Rev. Lett.* **60**, 1170 (1988).

²¹J. A. Jaszczak and D. Wolf, *J. Mater. Res.* **6**, 1207 (1991).

²²I. K. Schuller and A. Rahman, *Phys. Rev. Lett.* **50**, 1377 (1983).

²³C. L. Chien, S. H. Liou, and G. Xiao, in *Metallic Multilayers and Epitaxy*, edited by M. Hong, S. Wolf, and D. C. Gubser (The Metallurgical Society, New York, 1985), p. 245.

²⁴M. Komuro, Y. Kozono, S. Narishige, M. Hanazono, and Y. Sugita, *IEEE Trans. Magn. MAG-23*, 3701 (1987).

²⁵H. Doyama, M. Matsui, H. Matsuoka, S. Mitani, and K. Doi, *J. Magn. Magn. Mater.* **93**, 374 (1991).

²⁶H. Guo, X. Ma, L. Yang, B. Shen, and J. Zhao, *J. Magn. Magn. Mater.* **99**, 199 (1991).

²⁷H. Magnan, D. Chandesris, B. Villette, O. Heckmann, and J. Lecante, *Phys. Rev. Lett.* **67**, 859 (1991).

²⁸I. K. Schuller, *Phys. Rev. Lett.* **44**, 1597 (1980).

²⁹The relative compositions determined by inductively coupled plasma atomic absorption spectroscopy and x-ray diffraction are 2.8:1, 1:1.1, 1:2.1, and 1:3.3.

³⁰G. L. Eesley, B. M. Clemens, and C. A. Paddock, *Appl. Phys. Lett.* **50**, 717 (1987).

³¹K. A. Svinarich, W. J. Meng, and G. L. Eesley, *Appl. Phys. Lett.* **57**, 1185 (1990).

³²H. M. van Noort, F. J. A. den Broeder, and H. J. G. Draaisma, *J. Magn. Magn. Mater.* **51**, 273 (1985).

³³H. J. G. Draaisma, H. M. van Noort, and F. J. A. den Broeder, *Thin Solid Films* **126**, 117 (1985).

³⁴W. A. A. Macedo and W. Keune, *Phys. Rev. Lett.* **61**, 475 (1988).

³⁵P. A. Montano, G. W. Fernando, B. R. Cooper, E. R. Moog, H. M. Naik, S. D. Bader, Y. C. Lee, Y. N. Darici, H. Min, and J. Marcano, *Phys. Rev. Lett.* **59**, 1041 (1987).

³⁶S. C. Abrahams, L. Guttman, and J. S. Kasper, *Phys. Rev.* **127**, 2052 (1962); Y. Tsunoda, N. Kunitomi, and Y. M. Nicklow, *J. Phys. F* **17**, 2447 (1987).

³⁷G. W. Farnell, in *Physical Acoustics*, edited by W. P. Mason and R. N. Thurston (Academic, New York, 1969), Vol. 6, p. 109.

³⁸M. Grimsditch, *Phys. Rev. B* **31**, 6818 (1985); M. Grimsditch and F. Nizzoli, *ibid.* **33**, 5891 (1986).

³⁹D. Baral, J. E. Hilliard, J. B. Ketterson, and K. Miyano, *J. Appl. Phys.* **53**, 3552 (1982).